Journal of Power Sources 241 (2013) 572–577

Contents lists available at SciVerse ScienceDirect

Journal of Power Sources

journal homepage: www.elsevier.com/locate/jpowsour

Development of a 4.2 V aqueous hybrid electrochemical capacitor based on MnO_2 positive and protected Li negative electrodes

Wataru Shimizu [a], Sho Makino [a], Keita Takahashi [b], Nobuyuki Imanishi [b], Wataru Sugimoto [a,*]

[a] Faculty of Textile Science and Technology, Shinshu University, 3-15-1 Tokida, Ueda, Nagano 386-8567, Japan
[b] Faculty of Engineering, Mie University, 1577 Kurimamachiya-cho, Tsu, Mie 514-8507, Japan

HIGHLIGHTS

- An aqueous hybrid electrochemical capacitor is fabricated by using MnO_2 and Li.
- Electrodeposited MnO_2 has specific capacitance of 348 F g^{-1} at 2 mV s^{-1}.
- A pouched cell offers a 4.2 V cell voltage in a near-neutral aqueous electrolyte.
- A pouched cell has specific energy of 753 W h (kg MnO_2)$^{-1}$.
- Durability test shows an anticipated retention of 70% for 15,000 cycles.

GRAPHICAL ABSTRACT

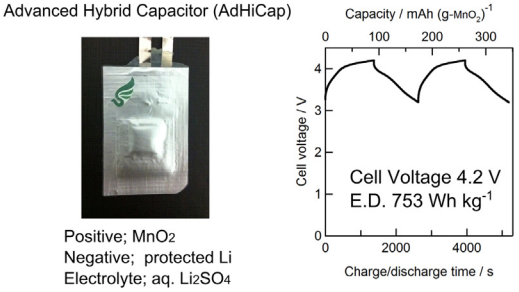

ARTICLE INFO

Article history:
Received 29 March 2013
Received in revised form
30 April 2013
Accepted 4 May 2013
Available online 14 May 2013

Keywords:
Electrochemical capacitor
Hybrid capacitor
Manganese oxide
Protected lithium anode

ABSTRACT

An aqueous hybrid electrochemical capacitor consisting of a capacitive manganese oxide (MnO_2) positive electrode and a water-stable, protected Li negative electrode in near-neutral aqueous electrolyte (1.0 M Li_2SO_4, pH = 5.5) is demonstrated. Galvanostatic charge/discharge cycling tests were conducted with pouched cells, offering a cell voltage of 4.2 V with maximum specific energy of 753 W h kg^{-1} based on the positive electrode. The combination of a pseudocapacitive MnO_2 positive and a Li negative electrode offers high specific charge and cell voltage, resulting in an aqueous hybrid electrochemical capacitor having exceptionally high specific energy.

1. Introduction

Electrochemical capacitors (ECs) are energy storage devices typically comprising of two porous electrodes and an aqueous or non-aqueous electrolyte, and are characterized by fast charge/discharge capability and long cycle life, thus being particularly suitable for energy harvesting [1,2]. ECs using aqueous electrolytes have several advantages compared to those using non-aqueous electrolytes including environmental friendliness, non-flammability and low cost. Typical electric double-layer capacitors using aqueous electrolyte are composed of carbon/carbon electrodes in symmetric configuration, delivering devices with energy densities of up to ~6 W h kg^{-1} and power densities of ~10 kW kg^{-1} [2–4]. The energy density E of ECs can be increased by increasing the capacitance C and/or cell voltage V, according to the formula $E = (1/2)CV^2$. Aqueous ECs have the advantage of being able to use high capacitance electrode materials, such as RuO_2 nanostructures (~700 F g^{-1}) [5,6]. Unfortunately, the operating voltage of aqueous ECs is limited by the thermodynamic 1.2 V water electrolysis voltage, generally resulting in

* Corresponding author. Tel.: +81 268 21 5455; fax: +81 268 21 5452.
E-mail address: wsugi@shinshu-u.ac.jp (W. Sugimoto).

0378-7753/$ – see front matter © 2013 Elsevier B.V. All rights reserved.
http://dx.doi.org/10.1016/j.jpowsour.2013.05.003

lower energy density compared to non-aqueous ECs based on carbon electrodes.

Aqueous ECs can be operated above 1.2 V by the use of positive electrode materials with high oxygen evolution overpotential, such as birnessite-type MnO_2 in combination with activated carbon as the negative electrode [7–9]. A 2.2 V aqueous EC in asymmetric cell configuration has been demonstrated by using sol–gel derived MnO_2 with 150 F g^{-1} as the positive electrode, producing a high energy density of 19 W h kg^{-1} based on the mass of active material in the electrode [10]. Despite the good electrochemical performance, the operating cell voltage needed to be limited to about 1.5 V for prolonged life to avoid hydrogen evolution at the activated carbon negative electrode.

In order to realize a high voltage aqueous device, hydrogen evolution at the negative electrode must be avoided. If the potential of the negative electrode can be lowered below the limit of the hydrogen evolution reaction, the extreme case would be the use of metallic lithium, cell voltage of over 4 V can be expected. Naturally, the lithium electrode cannot come in contact with the aqueous electrolyte. To fabricate an aqueous hybrid electrochemical capacitor exceeding 4 V, we have designed a novel aqueous system – Advanced Hybrid Capacitor (AdHiCap) – composed of porous positive electrodes and a water stable multi-layered Li negative electrode (protected Li electrode) [11]. The protected Li electrode, which has been developed for use as a negative electrode in Li–air rechargeable battery, is fabricated by sealing Li metal and a Li-ion conducting solid electrolyte with an aluminum package [12–14]. The AdHiCap combines the battery-like redox reaction at the Li negative electrode and capacitive charge storage at the positive electrode, similar to a lithium ion capacitor (LIC), which is a well-known hybrid EC with high cell voltage of ~4 V in non-aqueous electrolytes [15–17].

In our previous work, the proof-of-concept of AdHiCap was presented using chemically synthesized MnO_2 with acetylene black (AB) as a conductive additive in a beaker-type flooded cell setup [11]. A thin film electrode was utilized with glassy carbon as the current collector due to the poor electronic conductivity of MnO_2. MnO_2 prepared by electro-deposition [18–22] and sol–gel methods [10,23–25] have been reported to show specific capacitance ranging from ~130 F g^{-1} for powders [25,26] and ~400 F g^{-1} for thick films [20,22] to ~700 F g^{-1} for thin films [23,27] in near-neutral aqueous electrolytes. Electrodes prepared by electro-deposition generally lead to higher capacitance than sol–gel derived particles. In this work, to demonstrate a more practical cell configuration, thick MnO_2 positive electrodes are synthesized on carbon paper by anodic electro-deposition. Since MnO_2 can be synthesized directly on conductive carbon [20], conductive additives are unnecessary. Consequently, uniformity and electronic conductivity of MnO_2 electrodes are expected to be improved. Cell performance of AdHiCap is investigated by galvanostatic charge and discharge cycle tests with a beaker-type flooded cell in three-electrode configuration and a two-electrode pouched cell using near-neutral aqueous electrolyte. Consecutive cycling tests were also conducted on the pouched cell.

2. Experimental section

2.1. Materials

Manganese(II) sulfate pentahydrate ($MnSO_4 \cdot 5H_2O$, >99.9%), sulfuric acid (H_2SO_4, >97%), and lithium sulfate monohydrate ($Li_2SO_4 \cdot H_2O$, 99%) were purchased from Wako Pure Chemical Industries (Japan). Carbon paper (SIGRACET® GDL 10) was obtained from SGL Group (Germany). Lithium foil (0.2 mm thickness) was purchased from Honjo Metal (Japan). Nickel and copper foil (0.05 mm thickness) were purchased from Nilaco (Japan). Poly(ethylene oxide) (PEO, M_w; 6×10^5) and lithium bis(trifluoromethylsulfonyl)imide (LiTFSI, $Li(CF_3SO_2)_2N$) were purchased from Sigma–Aldrich (USA). Barium titanate was obtained from Sakai Chemical Industry (Japan). All chemicals were used as received.

2.2. Preparation of electrodes

Birnessite-type manganese oxide was electro-deposited on carbon paper (5 mm × 5 mm) according to the literature [20] and used as the positive electrode. A mixture of 1.0 M $MnSO_4 \cdot 5H_2O$ and 1.0 M H_2SO_4 in a 1:1 volume ratio was used as the electrolytic bath. Electro-deposition was conducted by applying a constant current density of 0.5 mA cm^2 for 600, 1200, 1800, 2700, 3600, or 5400 s at 25 °C. The deposited amount of MnO_2 was estimated from the difference in mass of the electrodes before and after electro-deposition using a microbalance (BM-252; AND, Japan).

The water-stable multilayered Li negative electrode was fabricated following previous studies [12–14]. A PEO film (ca. 300 μm thickness) containing LiTFSI and $BaTiO_3$ was placed between an LTAP glass ceramic (10 mm × 10 mm × 0.15 mm) and lithium foil (5 mm × 5 mm × 0.2 mm). The layered structure, Li/PEO–LiTFSI/LTAP, was sealed with aluminum packaging films under Ar gas atmosphere. A 5 mm × 5 mm window was cut out from one side of the aluminum package so that LTAP can be exposed to the aqueous electrolyte. Copper and nickel were used as the current collector for the positive and negative electrodes, respectively.

2.3. Characterization

Morphological features of the deposited MnO_2 were observed by using a S-5000 scanning electron microscope (Hitachi, Japan). To evaluate the electrochemical properties of the MnO_2 electrodes, cyclic voltammetry was conducted by using a three-electrode cell with a potentio/galvanostat (HZ-3000; Hokuto Denko, Japan). A platinum mesh was used as the counter electrode and a Ag/AgCl (saturated KCl) electrode was used as the reference electrode. Cyclic voltammetry was conducted between 0.6 and 1.6 V *vs.* RHE at scan rates of 500 to 2 mV s^{-1} in 1.0 M Li_2SO_4 deaerated with N_2 gas at 60 °C. The specific capacitance based on the mass of MnO_2 was calculated by averaging the anodic and cathodic charge obtained from the cyclic voltammograms. Charge and discharge curves were obtained from constant current cycling tests in beaker-type flooded cells consisting of the MnO_2 as the positive electrode, the protected Li electrode as the negative, and a Ag/AgCl reference electrode in the N_2-bubbled electrolyte solution. Current densities were varied between 0.04 and 1.2 mA cm^{-2}. Measurements were conducted at 60 °C to warrant sufficient ionic conductivity for LTAP (>10^{-4} S cm^{-1}) for electrochemical testing.

A pouched cell was fabricated by assembling the MnO_2 positive electrode, the protected Li negative electrode, and aqueous 1.0 M Li_2SO_4. The pouched cell can be represented as Li|PEO–LiTFSI|LTAP|1.0 M Li_2SO_4|MnO_2. The pouched cell was tested at 60 °C by galvanostatic charge and discharge cycles with a Bio-Logic VSP2 potentiostat. Consecutive cycling tests were conducted between 4.2 and 3.2 V at 0.6 mA cm^{-2}. Charge/discharge curves were periodically measured at 0.2 mA cm^{-2} during the cycling test. The specific energy was calculated by integration of the area of the discharge curve in a plot of cell voltage against capacity. Although the equation $(1/2)C(V_1 - V_2)^2$ is commonly used for calculating the energy density, this equation is not applied in this work to avoid overestimation of specific energy due to the slight non-linearity of the discharge curves.

3. Results and discussion

3.1. Half-cell evaluation of MnO_2 electrodes

Scanning electron microscopy images of the electro-deposited MnO_2 electrodes are shown in Fig. 1. The amount of MnO_2 grown on the carbon fibers increases with deposition time, with the morphology of the MnO_2 deposits changing from thin, flexible platelets to more rigid platelets. The carbon substrate was partially exposed with short deposition time of 600 s (Fig. 1(A)), while the entire carbon surface was covered for prolonged deposition time of 3600 s (Fig. 1(C)).

The mass of deposited MnO_2 was determined from the difference in mass of the electrodes before and after anodic electrodeposition using a microbalance (Fig. S1). To verify the accuracy of the measured mass, the deposited MnO_2 amount was also calculated using Faraday's law, $m = MIt/zF$, where m is the mass of the deposited MnO_2, M is the molecular weight of MnO_2 ($M = 86.94$ g mol^{-1}), I is the current passed, t is the deposition time, z is the electron number ($z = 2$), and F is the Faraday constant. In the case of the samples with deposition time $\leq$3600 s, the difference between the measured and calculated mass is within 8%. For longer deposition time, the mass calculated from the current passed tended to be slightly lower than that obtained using a microbalance. To avoid possible overestimation of the specific capacitance, the mass measured by microbalance will be applied.

Fig. 2 shows cyclic voltammograms of the MnO_2 electrodes prepared with deposition times of 600, 1800, and 3600 s in 1.0 M Li_2SO_4 electrolyte at 60 °C. The cyclic voltammograms slightly deform from the ideal rectangular shape for an ideally polarizable electrode for the thick MnO_2 electrode (3600 s) at high scan rates (Fig. 2(C)). The films obtained at longer electro-deposition times should have lower electronic and/or ionic conductivity caused by increasing thickness of MnO_2 platelets and dense morphology.

The specific capacitance at a low scan rate of 2 mV s^{-1} exhibited a maximum (348 F g^{-1}) at 1200 s deposition. At a high scan rate of 500 mV s^{-1}, the specific capacitance decreases to 92 F g^{-1} (Fig. S2). Fig. 3 shows the effect of electro-deposition time on the specific capacitance based on the mass of MnO_2 and the geometric surface area of the electrode at a scan rate of 2 mV s^{-1}. The capacitance normalized by the surface area increased continuously with increasing deposition time. The mass normalized capacitance exhibited a maximum at a deposition time of 1200 s, indicating that the increase in thickness of the individual MnO_2 platelets leads to lower utilization of the active material. The electrodes obtained with electro-deposition of 1800 s will be used hereafter.

3.2. Electrochemical characterization of MnO_2 positive and Li negative in flooded cell configuration

The electrochemical properties of the aqueous hybrid capacitor cell comprising of the MnO_2 positive electrode and the multilayered Li negative electrode in a flooded cell equipped with a Ag/AgCl reference electrode was studied. The voltage of the MnO_2 positive electrode was recorded versus the reference electrode with the protected Li electrode as the counter electrode at 0.2 mA cm^{-2} (Fig. 4). The charge/discharge curves of the protected Li electrode were obtained by subtracting the charge/discharge curves of the full cell from that of the MnO_2 positive electrode. The charge/discharge curves of the lithium negative electrode exhibited battery-like behavior between −2.8 V and −2.6 V *vs.* RHE, originating from the Li/Li$^+$ redox reaction. The charge/discharge curves of the MnO_2 positive electrode increased/decreased linearly with time, implying typical capacitive behavior. The *IR* drop for the full cell originates from the resistance of the protected Li negative electrode, as the *IR* drop at the MnO_2 positive electrode was small. The voltage drop of 0.124 V on discharge and 0.116 V on charge at 0.2 mA cm^{-2} can be translated to an equivalent series resistance (ESR) of 310 Ω cm^2 and 290 Ω cm^2, respectively.

3.3. Electrochemical capacitor behavior of pouched cell

A pouched cell was fabricated from the MnO_2 electrode and the protected Li electrode with 1.0 M Li_2SO_4 aqueous electrolyte. Charge and discharge curves of the pouched cell (Li|PEO–LiTFSI|LTAP|1.0 M Li_2SO_4 aq.|MnO_2) exhibited capacitive behavior between 3.2 and 4.2 V and were similar to that of typical LICs (Fig. 5(A)). The 4.2 V cell voltage was much higher than common aqueous hybrid capacitors ~2 V, owing to the low standard electrode potential of the protected Li electrode and the high overpotential for oxygen evolution of the MnO_2 positive electrode. The

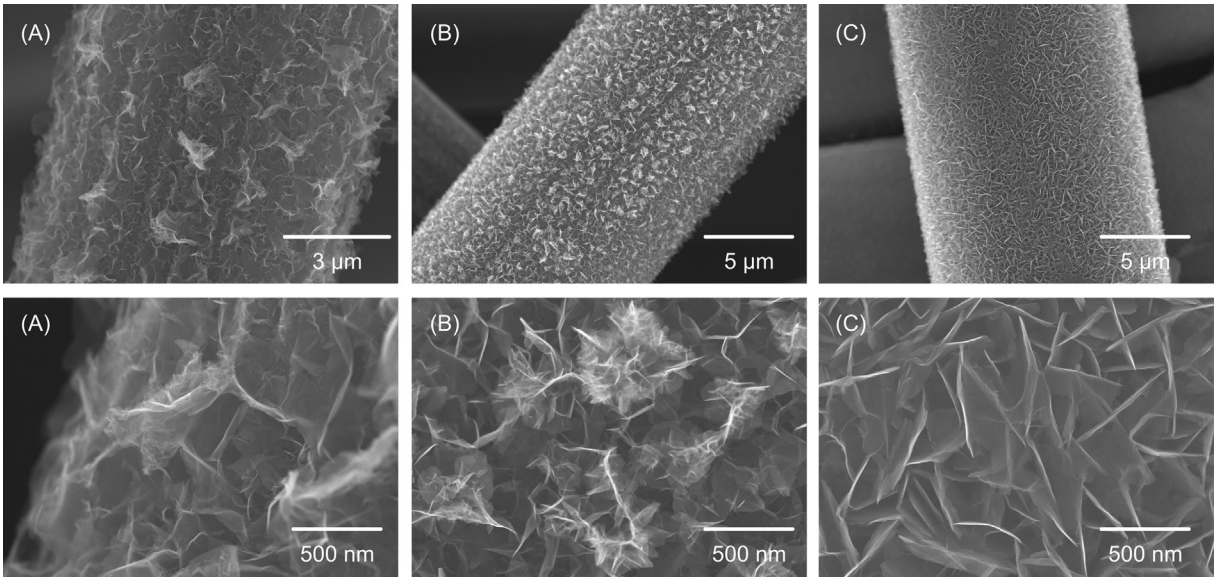

Fig. 1. Scanning electron microscopy images of the MnO_2 electrodes prepared with deposition time of 600 (A), 1800 (B), and 3600 s (C).

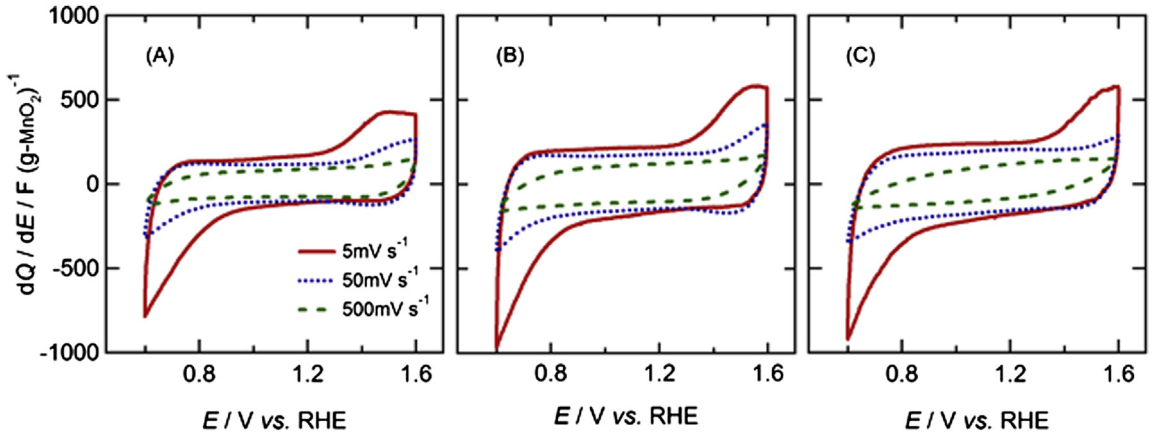

Fig. 2. Cyclic voltammograms of the MnO_2 electrodes synthesized with deposition time of 600 (A), 1800 (B), and 3600 s (C) at different scan rates of 5, 50, and 500 mV s^{-1} in 1.0 M Li_2SO_4 electrolyte at 60 °C.

cell voltage is even higher than EC devices operating in non-aqueous electrolytes, such as non-aqueous electric double-layer capacitors ($(C_2H_5)_4NBF_4$/acetonitrile; ~2.7 V) [28], ionic liquids (1-methyl-3-buthylimidazolium tetrafluoroborate; 3.5 V) [29], or commercial LICs (3.8 V) [30]. Discharge curves at high current density exhibited a linear change with time, typical of capacitive charge release (Fig. 5(B)). Non-linearity was obvious at low current density, which is in conjunction with the cyclic voltammograms. The equivalent series resistance evaluated from the *IR* drop of the discharge curve at 0.2 mA cm^{-2} (inset, Fig. 5(B)) was 244 Ω cm^2 in agreement with the values obtained from the flooded cell testing, and is in the same range as the resistance of the protected Li electrode obtained by impedance spectroscopy.

Specific capacity, energy, and power of the pouched cell (Li|PEO–LiTFSI|LTAP|1.0 M Li_2SO_4 aq.|MnO_2) are summarized in Table 1. The maximum specific capacity calculated from the discharge curve at 0.04 mA cm^{-2} was 201 mAh g^{-1} based on MnO_2, which translates to a specific energy of 753 W h kg^{-1}. Compared to our previous work in which sol–gel derived MnO_2 powder was used [11], a significant increase in performance was obtained by using electro-deposited MnO_2. The improved performance is attributed to the higher single electrode capacitance due to the different morphological character of chemically- or electrochemically-synthesized MnO_2. The mass of reacted lithium is estimated as 10.93 μg. From these values, the specific energy based on the mass of both electrodes (sum of the MnO_2 mass and reacted lithium) was 716 W h kg^{-1}. This value is 7 times higher than the state-of-the-art LIC of ~100 W h kg^{-1} based on mass of the active materials [16,17]. The high specific energy is attributed to the higher specific capacitance of the positive electrode and higher cell voltage.

The specific energy based only on the active material is a measure of the performance evaluation of electrode materials, and the mass and volume of other components (current collector, separator, electrolyte, binder, etc.) must be considered for a reasonable comparison in terms of practical applications [31]. Let us take for example, a factor of 1/12, which has been taken as a measure to translate the single-electrode specific energy per mass of carbon to a realistic energy density per mass of the practical device [31]. The maximum specific energy of 753 W h kg^{-1} and specific power of 4800 W kg^{-1} translates to 63 W h kg^{-1} and 400 W kg^{-1}, which is still about three times higher than commercial LICs of ~20 W h kg^{-1}. It should be emphasized that our laboratory-scale cell is far from optimized for practical device evaluation. Optimization of the current collector (carbon paper substrate), MnO_2 thickness, and reduction of ESR is expected to give even higher specific energy and power values.

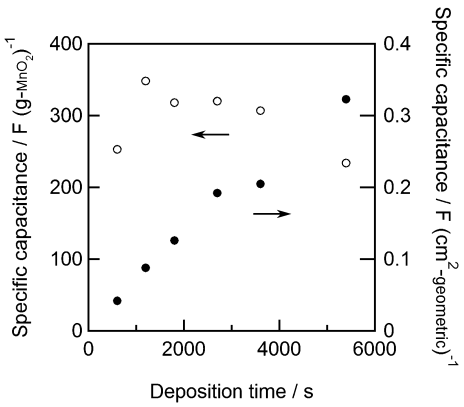

Fig. 3. The specific capacitance based on MnO_2 mass and geometric surface area at 2 mV s^{-1} as a function of the deposition time.

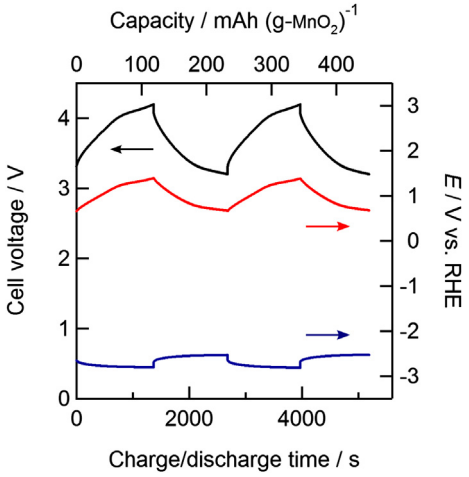

Fig. 4. Left axis: charge/discharge curves of the MnO_2 positive (1800 s deposition) and protected Li negative electrodes in flooded cell at 0.2 mA cm^{-2} (black). Right axis: charge/discharge curves of the MnO_2 positive electrode (red) and the Li negative electrode (blue) *vs.* RHE at 0.2 mA cm^{-2} (For interpretation of the references to color in this figure legend, the reader is referred to the web version of this article.).

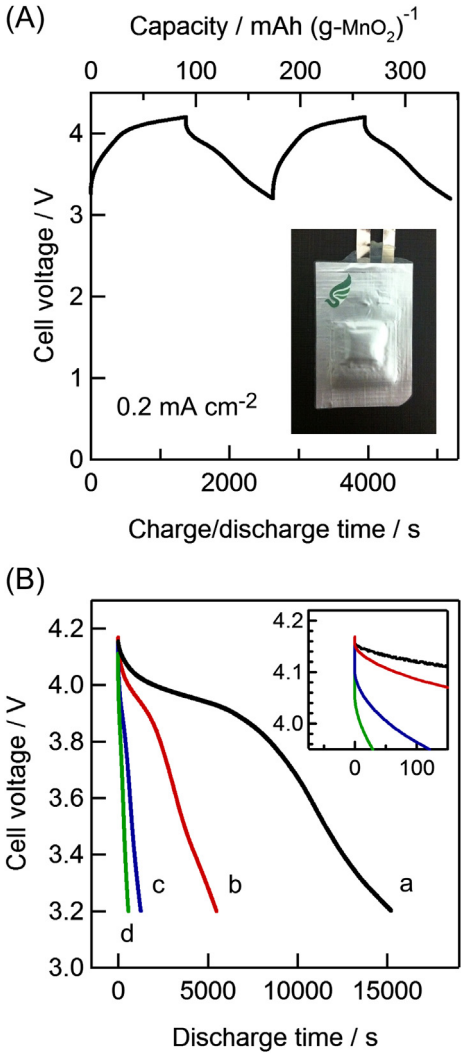

Fig. 5. (A) Charge/discharge curves of the pouched cell (Li|PEO–LiTFSI|LTAP|1.0 M Li_2SO_4 aq.|MnO_2) at 0.2 mA cm^{-2}. Inset in (A) shows a photograph of the fabricated pouched cell. (B) Discharge curves at different current densities with (a) 0.04, (b) 0.08, (c) 0.2, and (d) 0.3 mA cm^{-2}. The inset of (B) shows the magnified view of the curves at onset of discharge.

Consecutive charge/discharge cycle tests were conducted on the pouched cell at 0.6 mA cm^{-2}. The discharge curves at 0.2 mA cm^{-2} for cycle numbers 50, 200, 500, 1000, 1500, and 2000 are displayed in Fig. 6(A). After 2000 cycles, 85% of the specific energy obtained at the 50th cycle is retained (a loss of about 6 mW h kg^{-1} per cycle after the 200th cycle). Extrapolation of the data to 70% retention leads to an anticipated cycle life of 15,000 cycles.

Table 1
Selected properties of the pouched cell Li|PEO–LiTFSI|LTAP|1.0 M Li_2SO_4 aq.|MnO_2.

Current density/mA cm^{-2}	Specific capacity/ mA h g^{-1}			Specific energy/W h kg^{-1}			Specific power/ W kg^{-1}		
	Q_1[a]	Q_2[b]	Q_3[c]	E_1[a]	E_2[b]	E_3[c]	P_1[a]	P_2[b]	P_3[c]
0.04	201.0	191.1	16.8	753	716	63	178	169	15
0.08	145.0	139.8	12.1	533	514	45	350	337	29
0.2	83.0	81.3	7.0	300	294	25	860	840	72
0.3	55.8	55.0	4.7	200	197	17	1280	1260	110
0.4	39.4	39.0	3.3	139	138	12	1690	1670	140
0.6	22.7	22.6	1.9	79	79	7	2490	2480	210
0.8	15.3	15.2	1.3	53	53	4	3280	3270	280
1.2	7.7	7.7	0.6	26	26	2	4800	4830	400

[a] Normalized per mass of MnO_2.
[b] Normalized per mass of MnO_2 and Li used in discharge.
[c] Normalized per mass of MnO_2, carbon paper and Li used in discharge.

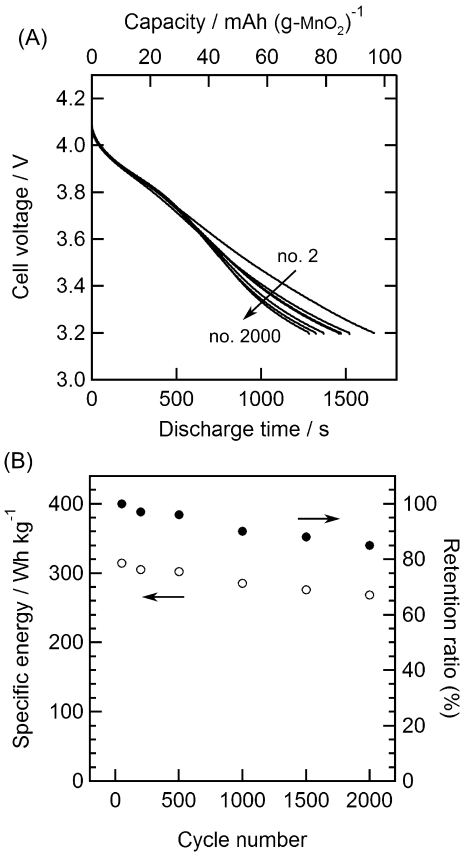

Fig. 6. (A) Discharge curves of the pouched cell (Li|PEO–LiTFSI|LTAP|1.0 M Li_2SO_4 aq.|MnO_2) at 0.2 mA cm^{-2} during the consecutive charge/discharge cycle test conducted at 0.6 mA cm^{-2}. (B) Specific energy and retention ratio as a function of the number of charge/discharge cycles.

4. Conclusions

A new aqueous electrochemical capacitor with a cell voltage of 4.2 V has been successfully demonstrated by combining MnO_2 with high overpotential for the oxygen evolution and a protected Li electrode. Thick MnO_2 electrodes were fabricated by anodic electro-deposition on carbon paper. Charge/discharge curves of the pouched cell indicated typical capacitive behavior between 4.2 and 3.2 V. Detailed examinations in a flooded-cell configuration equipped with a reference electrode clarified capacitive charge and discharge at the positive MnO_2 electrode and battery-like redox behavior at the protected Li negative electrodes. The high cell voltage and specific capacity offered by the pseudo-capacitive charge storage of MnO_2 in 1.0 M Li_2SO_4 (pH ≈ 5.5) ensured high specific energy of 716 W h kg^{-1} based on the mass of MnO_2 and Li, which is 7 times higher than the state-of-the-art LIC of ~100 W h (kg carbon)$^{-1}$. The tested cell still has much room for improvement, especially in terms of energy per unit volume. The volumetric energy of the present cell is small since the carbon paper at the positive electrode occupies a large volume of pouched cell. Nonetheless, the present aqueous hybrid capacitor has many advantages, such as its environmental friendliness and non-flammability compared to organic electrolyte systems. Although this research is still in a preliminary stage, the high cell voltage and specific energy derived from AdHiCap promises to pave the way to next generation capacitor/battery technology.

Acknowledgments

This work was supported in part by the Advanced Low Carbon Technology Research and Development Program (ALCA) of the Japan Science and Technology Agency (JST).

Appendix A. Supplementary data

Supplementary data associated with this article can be found in the online version, at http://dx.doi.org/10.1016/j.jpowsour.2013.05.003.

References

[1] M. Conte, Fuel Cells 10 (2010) 806.
[2] J.W. Long, D. Bélanger, T. Brousse, W. Sugimoto, M.B. Sassin, O. Crosnier, MRS Bull. 36 (2011) 513.
[3] Y. Zhai, Y. Dou, D. Zhao, P.F. Fulvio, R.T. Mayes, S. Dai, Adv. Mater. 23 (2011) 4828.
[4] J. Garche, C. Dyer, P. Moseley, Z. Ogumi, D. Rand, B. Scrosati, Encyclopedia of Electrochemical Power Sources, vol. 1, Elsevier, Amsterdam, 2009, pp. 607–633.
[5] J.P. Zheng, P.J. Cygan, T.R. Jow, J. Electrochem. Soc. 142 (1995) 2699.
[6] W. Sugimoto, H. Iwata, Y. Yasunaga, Y. Murakami, Y. Takasu, Angew. Chem., Int. Ed. Engl. 42 (2003) 4092.
[7] J. Jiang, A. Kucernak, Electrochim. Acta 47 (2002) 2381.
[8] M.S. Hong, S.H. Lee, S.W. Kim, Electrochem. Solid-State Lett. 5 (2002) A227.
[9] Y.U. Jeong, A. Manthiram, J. Electrochem. Soc. 149 (2002) A1419.
[10] T. Brousse, M. Toupin, D. Bélanger, J. Electrochem. Soc. 151 (2004) A614.
[11] S. Makino, Y. Shinohara, T. Ban, W. Shimizu, K. Takahashi, N. Imanishi, W. Sugimoto, RSC Adv. 2 (2012) 12144.
[12] S. Hasegawa, N. Imanishi, T. Zhang, J. Xie, A. Hirano, Y. Takeda, O. Yamamoto, J. Power Sources 189 (2009) 371.
[13] T. Zhang, N. Imanishi, S. Hasegawa, A. Hirano, J. Xie, Y. Takeda, O. Yamamoto, N. Sammes, Electrochem. Solid-State Lett. 12 (2009) A132.
[14] T. Zhang, N. Imanishi, Y. Shimonishi, A. Hirano, J. Xie, Y. Takeda, O. Yamamoto, N. Sammes, J. Electrochem. Soc. 157 (2010) A214.
[15] G.G. Amatucci, F. Badway, A. Du Pasquier, T. Zheng, J. Electrochem. Soc. 148 (2001) A930.
[16] V. Khomenko, E. Raymundo-Piñero, F. Béguin, J. Power Sources 177 (2008) 643.
[17] S.R. Sivakkumar, A.G. Pandolfo, Electrochim. Acta 65 (2012) 280.
[18] Y.-C. Chen, Y.-K. Hsu, Y.-G. Lin, Y.-K. Lin, Y.-Y. Horng, L.-C. Chen, K.-H. Chen, Electrochim. Acta 56 (2011) 7124.
[19] C.-C. Hu, T.-W. Tsou, Electrochem. Commun. 4 (2002) 105.
[20] M. Wu, G.A. Snook, G.Z. Chen, D.J. Fray, Electrochem. Commun. 6 (2004) 499.
[21] O. Ghodbane, J.-L. Pascal, F. Favier, ACS Appl. Mater. Interfaces 1 (2009) 1130.
[22] C.-C. Hu, C.-Y. Hung, K.-H. Chang, Y.-L. Yang, J. Power Sources 196 (2011) 847.
[23] S.-C. Pang, M.A. Anderson, T.W. Chapman, J. Electrochem. Soc. 147 (2000) 444.
[24] M. Toupin, T. Brousse, D. Bélanger, Chem. Mater. 14 (2002) 3946.
[25] R.N. Reddy, R.G. Reddy, J. Power Sources 124 (2003) 330.
[26] M. Toupin, T. Brousse, D. Bélanger, Chem. Mater. 16 (2004) 3184.
[27] S.-F. Chin, S.-C. Pang, M.A. Anderson, J. Electrochem. Soc. 149 (2002) A379.
[28] B.E. Conway, Electrochemical Supercapacitors: Scientific Fundamentals and Technological Applications, Springer, New York, 1999.
[29] K.K. Denshchikov, M.Y. Izmaylova, A.Z. Zhuk, Y.S. Vygodskii, V.T. Novikov, A.F. Gerasimov, Electrochim. Acta 55 (2010) 7506.
[30] K. Naoi, S. Ishimoto, J. Miyamaoto, W. Naoi, Energy Environ. Sci. 5 (2012) 9363.
[31] Y. Gogotsi, P. Simon, Science 334 (2011) 917.